The Pennsylvania State University

The Graduate School

Department of Mechanical and Nuclear Engineering

CHARACTERIZATION OF HEAT TRANSFER COEFFICIENT AT MICRO/NANO SCALE AND THE EFFECT OF HEATED ZONE SIZE

A Thesis in

Mechanical Engineering

by

Raghu Surya Rama Abhilash Pulavarthy

Submitted in Partial Fulfillment
of the Requirements
for the degree of

Master of Science

August 2015

The thesis of Raghu Pulavarthy was reviewed and approved* by the following:

Aman Haque
Professor of Mechanical Engineering
Thesis Adviser

Tak Sing Wong
Assistant Professor of Mechanical Engineering

Karen A. Thole
Professor of Mechanical Engineering
Head of the Department of Mechanical and Nuclear Engineering

* Signatures are on file in the Graduate School

ABSTRACT

Heat transfer mechanism from hot solids to surrounding air is crucial in thermal systems. Thermal management of devices at micro/nano length scales is very important for their reliability as they continue to shrink in size. It is agreed widely that the heat transfer coefficient increases at smaller length scales. This work presents an experimental technique to characterize the heat transfer from micro and nano scale structures using infrared microscopy. The heat transfer coefficient is found to be two orders of magnitude higher than the value at bulk length scales. It also shows an inverse relationship with temperature of the solid which suggests that the solid to air conduction is the dominating mechanism of heat dissipation at small length scales. An empirical relationship is also presented that depends on ratio of surface area to cross-sectional area, temperature differential in the heated solid and its surroundings. The heat transfer coefficient in conjunction with the temperature map from the infrared microscope can be used to measure the thermal conductivity of specimen using a heat transfer model based on micro fin geometry.

It is assumed that this size effect on the heat transfer coefficient is due to the size of specimen. An experiment is presented to show the effect of the predominance of the heater size on the heat transfer coefficient. For micro-heaters, the heat transfer coefficient is measured to about 3200 W/m^2 K. This value drops to about 110 W/m^2 K for a millimeter scale heater and to 10 W/m^2 K for a macroscopic heater; all for a nanoscale thin film specimen.

TABLE OF CONTENTS

List of Figures

List of Tables

Acknowledgement

I will be highly indebted to my graduate advisor, Dr. Aman Haque who has been mentoring me with his constant guidance and positive criticism of all my shortcomings. His supervision of my research work made sure I am heading in the right direction. I also thank Dr. Tak Sing Wong for agreeing to be the faculty reader of my thesis and be ready to help me. Special thanks to my colleagues Tarek and Baoming for helping me in getting acquainted with various fabrication and microscopy tools and providing moral support. It would be unfair if I don't acknowledge the support provided by the staff at the Nanofab, the MCL and the ADL at Binghamton – Guy, Shane, Mike, Kathy, Tim, Andy, Bangzhi, Josh, Trevor and Intae. A sincere gratitude to my housemates and friends who made sure I had a proper work balance and also stood by me during the stressful times. Last but not the least, utmost thanks goes to my parents, grandparents and sister for being a constant source of encouragement and having belief in me

1. Introduction

The mechanism of heat transfer from hot solids to the surrounding environment is crucial in wide variety of thermal systems [1]. The literature is particularly rich for bulk scale free and forced convective heat transfer but comparatively very little is known at the micron and submicron scales. This is critical for operation and reliability of micro-electronic and micro-electro-mechanical systems, where rapid and ever continuing miniaturization results in very high power dissipation densities [2]. The physics of solid to gas heat transfer changes considerably at length scales [3-6] that are on the same order of certain characteristic length parameters of the medium of heat transfer. Devices at these lengths are now routinely designed for applications like integrated circuits, heated cantilever thermometry [4], gas based sensors [7, 8] and micro-actuators [6] for which accurate prediction of free convective heat transfer is of paramount importance.

At the macroscale, the bulk flow (either due to density variation or externally imposed) of the fluid surrounding a heated solid is responsible for convective heat transfer. At the bulk scale, the heat transfer coefficient is a weak function of the temperature of the heated solid, which diminishes at higher temperatures. Pressure also influences the heat transfer coefficient since the molecular density of air is pressure dependent. A second mode of heat transfer is through diffusion and/or conduction at the still boundary layers next to the solid. Maxwell [9] introduced the concept of molecular conduction in gases. The thermal conductivity was derived to be proportional to the specific heat at constant volume, density, mean free path and the mean velocity of molecules. Since the density is directly and the mean free path is inversely proportional to the number of molecules per unit volume, dependence of the mean velocity is decisive, if the specific heat can be taken as constant. Thus thermal conductivity does not depend on pressure or density and is proportional to the square root of temperature. This is very different from the classical notion of advection dominated heat transfer. Therefore, the relative contribution from the two mechanisms, advection and molecular conduction, determines the nature of the temperature and pressure dependence of the heat transfer coefficient.

While for macroscale objects, density difference drives the flow associated with natural convection, the buoyancy forces at the smaller scales are too small to strongly overcome the forces of viscous drag which oppose the convective motion. When a heated microstructure is suspended in air, the dominant mode of heat transfer is conduction through the air, and natural convection at such microscale devices is less important as evident from literature [3, 10]. Due to the small size of the system, density variations are very small in the control volume, and thus gravitational forces do not become significant. This shows that at the microscale, the classical notion of advection may not be dominant and conduction should be considered [11, 12]. Hu et al. [10] studied heat transfer from an aluminum micro heater fabricated on a silicon nitride thin film using 3ω measurements. Guo et al. [13] investigated the size effect on heat transfer in micro devices. These studies suggest that larger surface area to volume ratio in the heated solid will have an impact on heat transfer coefficient. It is also argued that the natural convection is less significant in a micro-enclosure owing to very small buoyancy, which is the driving force. The Grashof number is estimated, assuming the side surface of the silicon beam as a vertical flat plate that is 20 μm long, to be in the order of 10^{-5}, which again reinforces the observation that buoyancy forces can be neglected when compared to viscous forces.

The rapid advances in miniaturization, particularly in thermal sensors, mechanical actuators, electrical current switches and all other heat dissipating devices, has resulted in renewed interest in size effects on heat transfer. While solid to gas heat transfer at micron and submicron scales remains an open area for research, the general consensus from the existing studies is that the heat transfer coefficient (h) increases with decreasing length scale. The value of h for bulk scale free convection is generally within the range of 10-25 W/m^{2}K. A simple scaling argument using the correlation between Nusselt, Rayleigh and Prandtl numbers let Peirs et al. [6] suggest h value in the order of 100 W/m^{2}K for air at length scales around 100 μm. Kim [4] studied heat transfer between a micro cantilever with an integrated heater at the top and surrounding air using continuum finite element simulations. The calculated effective heat transfer coefficient around the heater portion and cantilever leg is considerably large; around 7000 W/m^{2}K near the heater and 1000 W/m^{2}K near the cantilever base. Giani et al. [14] presented a thermal model of a silicon rich silicon nitride thin film anemometer with a platinum heater. It is shown that the convection is dominating compared to conduction and radiation. Thermal conductance was calculated due to various modes of heat transfer and deducted the value of heat transfer coefficient to be in the order of 200 W/m^{2}K. Wang et al. [5] studied the heat transfer around a platinum micro-wire using the 3ω method and reported heat transfer coefficient values ranging from 100-1000 W/m^{2}K depending on the diameter of the micro-wire. The degree of variation (100-7000 W/m^{2}K) in the literature suggests that the heat transfer coefficient is strongly influenced not only by size but also on other factors that may not have been addressed consistently across the existing studies, which provides motivation for the current study. Most of the existing literature attempts to measure the microscale heat transfer coefficient as a unique value, whereas a comprehensive study should involve the influence of temperature and pressure. Cheng et al.[12] measured the heat transfer coefficient between a free standing VO_2 nanowire and quiescent surrounding air using laser thermography and found that the coefficient is strongly dependent on pressure above ~10 Torr unlike that observed for macroscale solids, where it is pressure independent. Very little work has been done to measure the dependence of heat transfer coefficient on parameters like temperature and pressure [15, 16] at micro and nano scales. This motivates the present experimental study, which is aimed at measuring the heat transfer coefficient at small scales and exploring its dependence on temperature and pressure.

2. Methodology

In this study, a micro device is designed and fabricated that integrates a micro heater with a free standing specimen using standard nanofabrication techniques. The specimen is essentially a heavily doped single crystal silicon beam, 10 μm wide and 20 μm thick. To study the dimensional sensitivity on the heat transfer coefficient, a 100 μm segment was photo-lithographically reduced to 8 μm X 20 μm in cross-sectional size. Further reduction in cross-section size to 8 μm X 1 μm was performed with focused ion beam milling. Figure 2.1 shows a scanning electron micrograph (SEM) image of the micro device, highlighting the different parts. The size of the entire device is 3 mm X 5 mm and is compatible with scanning electron, probe or infrared microscopy. The nanofabrication process starts with patterning photo resist on a SOI wafer (20 μm thick highly doped single crystal device layer silicon, 2 μm buried oxide and 400 μm handle layer silicon) by photolithography, as shown in Figure 2.2. The device layer is then etched by an anisotropic Deep Reactive Ion Etch (DRIE) process. Sample specimens are then exposed to hydrofluoric acid vapor to remove the 2 μm oxide between the silicon layers and eventually release the device layer features from the floor i.e., handle layer silicon. In a separate batch of devices, a backside lithography and DRIE was used to remove the entire handle layer beneath the specimen. Finally, the resist is stripped off by using oxygen plasma. The specimen was designed to have a narrow cross-section (8 μm X 20 μm) compared to the remaining values of 10 μm X 20 μm. After the device is fabricated, a small part of the 20 μm thick silicon sample beam is milled away using a Focused Ion Beam (FIB) to create 8 μm X 1 μm cross-section and 12 μm long constricted region as shown in Figure 2.1a.

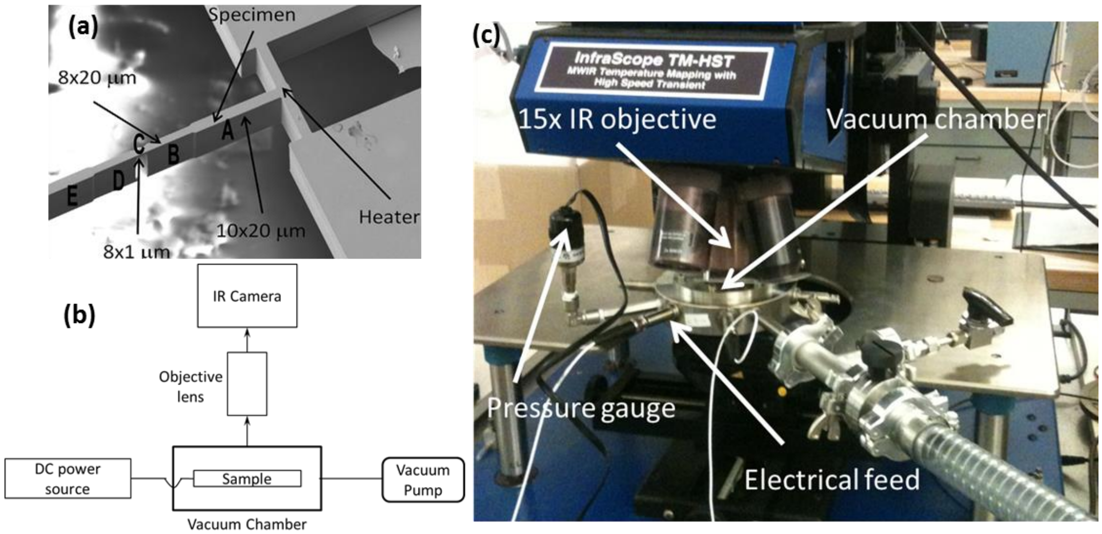

Figure 2.1 (a) Scanning Electron Micrograph of the device with specimen and T-heater (b) Schematic and (c) Optical image of the Experimental Setup showing infrared microscope and vacuum chamber

2.1 Experimental Procedure

A typical experiment starts with the passage of known electrical current through the heater beam (Figure 2.1a) while the device is in atmospheric pressure and room temperature. As current is passed through the heater, which generates heat due to Joule heating, a parabolic temperature profile is developed along the length of heater owing to symmetry. The highest temperature is observed in the middle of the heater beam where it intersects with the sample specimen, thereby conducting heat to create a temperature gradient along the length of the sample. A temperature gradient in the transverse direction also exists, with high temperature at the specimen surface and exponentially decaying to the ambient temperature in the surrounding air. The temperature distribution is measured using Infrascope II thermal microscope (Quantum Focus Instruments Corporation) with spatial and temperature resolution of about 1.6 μm and 0.1° K respectively. Once the temperature distribution is recorded for the initial electrical current through the heater (starting with 20 mA), the current is progressively increased by 5 mA and thermal images are recorded for each value of electrical current until it reaches 80 mA. A vacuum chamber with

CaF_2 viewport and electrical feed-through (as shown in Figure 2.1b) is also developed so that the experiments could be carried out in a controlled vacuum environment. The device is then placed inside the vacuum chamber and electrical connections are completed via feed-through. After the chamber is pumped down to moderately low vacuum (3 Pa), thermal images are collected for the same set of electrical current values. All the thermal images are recorded in the steady state limit i.e., when no changes in temperature with time are observed in the microscope.

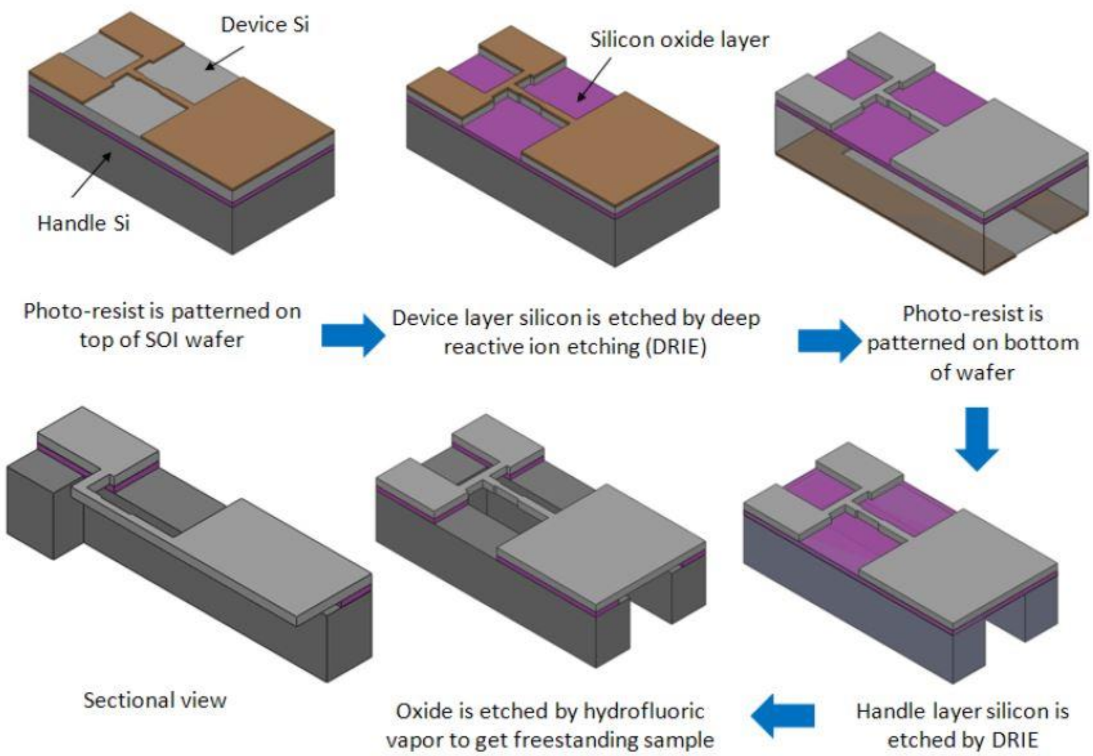

Figure 2.2 Nanofabrication processing steps for the micro device containing the specimen and micro heater

2.2 Mathematical Model

2.2.1 Determination of Heat Transfer Coefficient

The heat transfer coefficient in quiescent air medium can be obtained by two different ways. The first technique utilizes the heating (or cooling) timescale, in conjunction with mass (m), surface area (S) and specific heat c_p, as given in the following equation [17],

$$h = \frac{rmc_p}{S} \tag{2.1}$$

The term r is the inverse of the time constant for the object, which is obtained from curve fitting the time dependent temperature data that typically follows an exponential profile,

$$T = T_\infty + [T(0) - T_\infty]e^{-rt} \tag{2.2}$$

While the transient mode temperature measurement in our experimental setup can achieve micro-second resolution, the exact mass measurement is difficult for the specimen under study. This is due to the inherent temperature gradient in the sample specimen. The second technique is to perform an energy balance between conduction in the specimen accounting for the convective heat losses. This technique requires measurement of the temperature profile in the vicinity of the heated solid surface. In this study, we measured the temperature profile across the sample to infer the air boundary layer temperature with infrared thermal microscopy. Infrared thermography has been a powerful tool for macroscopic convective heat transfer measurement [18, 19]. Figure 2.3a shows an image obtained from the thermal microscope. The lateral T(y) scan operation, done at any section of the silicon beam, gives the temperature variation with distance away from the surface. An exponential distribution in space is suggested as the best fitting function by Roldan et al. [20] to allow T (air temperature at position y) to approach the room temperature T_∞ as $y \rightarrow \infty$.

$$T = T_\infty + [T_w - T_\infty]e^{-sy} \quad (2.3)$$

Where T_w is the wall temperature of the specimen at the interface with surrounding air and s is a constant determined by plotting the logarithm of the temperature against the distance (y) from the specimen surface at temperature T_w.

$$\ln \frac{T - T_\infty}{T_w - T_\infty} = s * y \quad (2.4)$$

The boundary condition that the air just adjacent to the surface is at rest and conducts heat by pure diffusion relates the temperature to the thermal conductivity of the air. The conductive heat flux Q given by the Fourier's law of conduction is

$$Q = -k_{air} \frac{dT}{dy}\Big|_{surface} \quad (2.5)$$

where k_{air} is the thermal conductivity of air. The local heat transfer coefficient is defined as

$$h = \frac{Q}{(T_w - T_\infty)} \quad (2.6)$$

On substituting the conductive flux at the surface, we obtain the expression for the local heat transfer coefficient as

$$h = k_{air} * s \quad (2.7)$$

2.3 Experimental Results and Validation

2.3.1 Experimental Results

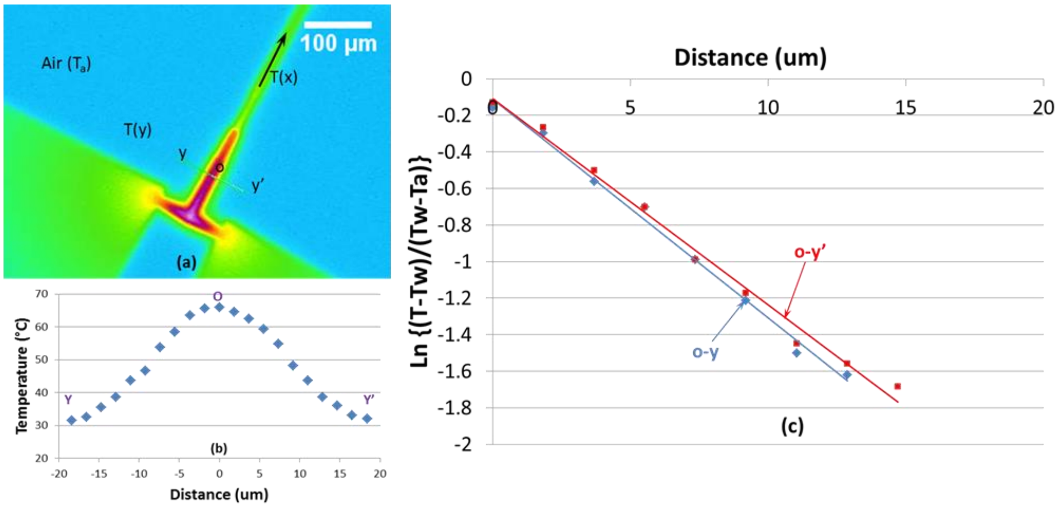

Figure 2.3 (a) Infrared micrograph of the specimen, (b) Temperature profile along the y-0-y' line in (a) and (c) Determination of the exponent s in Equation 2.3

Figure 2.3a shows the image from the thermal microscope when 60mA current is passed through the heater. The green line (y-y') perpendicular to the length of the beam shows the section of the lateral scan for which the temperature variation with length is shown in Figure 2.3b. According to Equation 2.4, the plot of $\ln \frac{T-T_\infty}{T_w-T_\infty}$ and y should be linear with slope s. This is shown in Figure 2.3c. Similar line scans are performed at different sections along the length of the beam, which are at different temperatures because the specimen is heated only from one end. This allows us to measure the heat transfer coefficient at various specimen temperatures. Figure 2.4 shows a plot for both the temperature profile of the specimen and the measured heat transfer coefficient at different locations labeled from A to E. The heat transfer coefficient obtained by this technique is about two orders of magnitude higher than that for macroscopic bodies. Also evident is the strong dependence of h with temperature, which varies by approximately 25% within a very small temperature differential of 35° C. This is not explained by the bulk motion of the fluid particles being the dominant contribution in the convection. It is to be noted that the results discussed in this section are for the experiment carried out at atmospheric pressure.

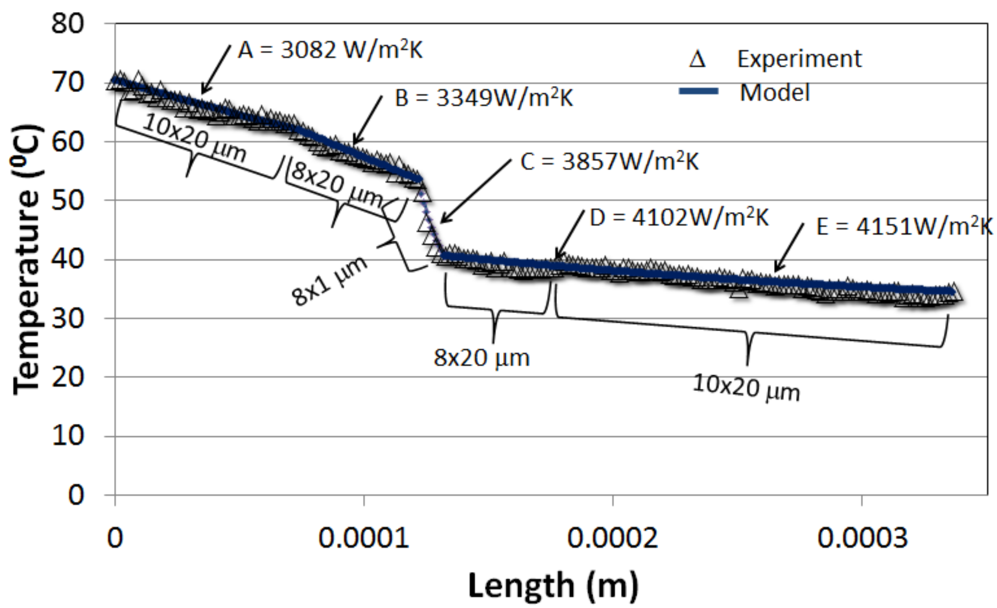

Figure 2.4 Temperature profile along the sample specimen showing the measured heat transfer coefficient at different locations

The boundary layer thickness and the heat transfer coefficient obtained for the microstructure are compared with those for a bulk scale object and are calculated using the following correlations:

$$\delta_{th,H} = 5H\left(\frac{Gr_H}{4}\right)^{-1/4} \tag{2.8}$$

$$\overline{Nu_H} = \left[0.68 + \frac{0.670 Ra_H{}^{1/4}}{\left[1+(0.492/Pr)^{9/16}\right]^{4/9}}\right] \tag{2.9}$$

where $\delta_{th,H}$ is the boundary layer thickness of a vertical flat plate of length H, Gr_H is the Grashof number, Nu_H is the Nusselt number, Ra_H is the Rayleigh number and Pr denotes the Prandtl number of air. In order to observe the effect of pressure on the temperature dependence of heat transfer coefficient, an experiment was conducted in a moderate vacuum (3 Pa) and the results are compared with those in ambient pressure.

Table 2.1 Comparison of bulk and micro scale convective heat transfer

H_{char} [m]	Grashof No.	$\delta_{th,H}$ [m]	Nusselt No.	δ_{th}/H_{char}	h [W/m^{2}K]
20.0E-02 (bulk)	2.0963E+07	2.348E-02	32.534	8.51	4.47
20.0E-06 (micro)	2.0963E-05	2.348E-03	0.711	117.43	979.54

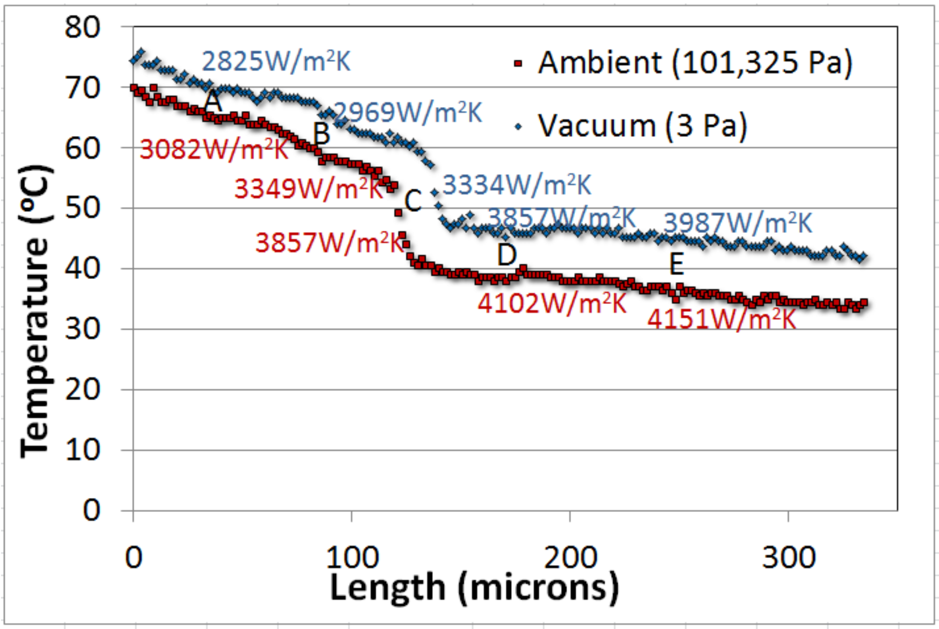

Figure 2.5 Temperature profile of the silicon specimen at two different pressures

As can be seen in Figure 2.5, the temperature of the specimen is relatively higher in vacuum because of the reduced heat loss through convection. Nevertheless, the apparent temperature dependence of h remains the same. The higher temperature of the specimen can be explained by the low molecular density and high inter-molecular space in the surrounding air. It makes the heat transfer through diffusion process less prominent and hence the reduced heat transfer coefficient values. The decrease of h varies approximately from 4-8% in the total length of the specimen beam.

2.3.2 Validation of the Experimental Results

In order to validate the experimentally obtained values of the heat transfer coefficient, a model is developed to evaluate the temperature of the silicon beam from the first law of thermodynamics. An energy balance is performed at the specimen surface to measure the heat transfer coefficient. These measurements are validated by using the values in calculating the thermal conductivity (or in other words, the temperature gradient along the specimen length), because the thermal conductivity of silicon is very well characterized in the literature [17].

$$\frac{\partial E_{CV}}{\partial t} = \dot{E}_{in} - \dot{E}_{out} + \dot{E}_{gen} \quad (2.10)$$

Since there is no internal heat generation ($\dot{E}_{gen}$) in the specimen, at steady state, heat incoming ($\dot{E}_{in}$) to a control volume is balanced by the outgoing heat ($\dot{E}_{out}$) in form of conduction, convection and radiation. The heat loss, dq_{out}, by convection and radiation can be written as

$$dq_{out} = h * dS * (T - T_{\infty}) + \varepsilon * \sigma * dS * (T^4 - {T_{\infty}}^4) \quad (2.11)$$

Where ε is the emissivity of air, σ is Stefan–Boltzmann constant and dS is the surface area of the differential control volume. For small temperature differences, Equation 2.11 can be approximated as

$$dq_{out} = (h + \varepsilon * \sigma * 4{T_{\infty}}^3) * dS * (T - T_{\infty}) \quad (2.12)$$

$$dq_{out} = \left(h_{approx}\right) * dS * (T - T_{\infty}) \quad (2.13)$$

Equation (2.13) with boundary conditions and experimentally obtained values of heat transfer coefficient is used to validate the temperature of the silicon beam along its length. The temperature distribution is then developed by approximating the silicon beam as an extended surface with a constant temperature boundary condition at x=L [17].

$$\frac{\Theta}{\Theta_b} = \frac{\frac{\Theta_L}{\Theta_b}\sinh mx + \sinh m(L-x)}{\sinh mL} \qquad (2.14)$$

where Θ = T-T_∞, $\Theta(0) = \Theta_b$, $\Theta(L) = \Theta_L$ and $m^2 = \frac{h_{approx}P}{kA_c}$. The h values measured previously (locations A-E in Figure 2.4) are used in the above expression. P is the perimeter of cross-sectional area A_c of the beam. Figure 2.4 also shows the predicted temperature distribution along the length of the specimen for thermal conductivity of 140 W/mK, which shows a remarkable fit between the measured and predicted temperature profiles. Since the thermal conductivity (k) of silicon is very well known in the literature, Figure 2.4 convincingly validates the measured values of the heat transfer coefficient.

2.3.3 Experimental Uncertainty Analysis

Using equations 2.4 and 2.7, the uncertainty analysis has been carried out. The expression for the uncertainty in evaluating the heat transfer coefficient due to the associated uncertainties in measured quantities is

$$\frac{\Delta h}{h} = \frac{\Delta y}{y} + \frac{2\Delta T}{\ln\left(\frac{T-T_\infty}{T_w-T_\infty}\right)}\frac{1}{(T-T_\infty)}\left[1-\frac{T-T_\infty}{T_w-T_\infty}\right] \qquad (2.15)$$

It is to be noted that the spatial resolution mentioned earlier is not the uncertainty in measuring y. The output of the thermal microscope is a pixel by pixel temperature plot. For a certain magnification, the pixel to pixel distance is a fixed number and is not the error bar of y. A relative error of 10% in y is assumed which is a reasonable approximation. This gives a relative uncertainty of 10-11% in the heat transfer coefficient as evaluated using Equation 2.15.

2.4 Discussion

In this study, the heat transfer coefficient is measured by conducting the experiments on microscale specimens. The experimental results are in the same order of magnitude with the values given by Kim et al.[4]. The results also show pronounced effect of specimen temperature previously not reported in the literature. The observed large values of the heat transfer coefficient can be related to the thickness of the thermal boundary layer developed in the vicinity of the specimen surfaces. Since the characteristic length of the device is in the order of tens of micrometer (Kn ~ 0.001), the assumption of flow continuum is valid.

Table 2.1 compares the heat transfer characteristics of a micro (present study) scale and a macroscale object. The Grashof number for the specimens in this study is very small, which reinstates the argument that the buoyancy forces are negligible at low length scales. The boundary layer is more compressed and the heat transfer coefficient obtained is in the same order of magnitude with that presented by Piers et al. [6]. Such a high heat transfer coefficient in the absence of bulk fluid motion (very little buoyancy) explains the heat diffusion through air molecules is the major mechanism of energy transfer. This implies that these correlations are mostly dominated by thermal conduction and not affected by the advection and agrees with Kim et al.[4]. This also supports the observed pronounced temperature dependence. At lower temperatures, the air molecules in the thermal boundary layer have lower kinetic energy and consequently are capable of higher rates of heat transfer by diffusion. This phenomenon is pronounced by the relative thickness of the thermal boundary layer at the microscale. As seen in

Table 2.1, the ratio of δ_{th}/H_{char} is more than an order of magnitude larger at the microscale compared to the bulk. Considering the dominance of heat conduction through the air surrounding the specimen, the relative thickness of the boundary layer can play significant role in the effective heat transfer. In other words, the relative thermal boundary layer thickness at the bulk scale is too thin to show any appreciable effect of temperature on the kinetic energy of the air molecules inside the boundary layer. This explains the relative temperature insensitivity of the heat transfer coefficient at the macroscale.

Such high heat transfer coefficient value makes the convective heat transfer from microscale objects to the surrounding air comparable to that through the specimen. We therefore propose that at the microscale, the ratio of specimen surface area S (solid to fluid medium heat transfer) to the cross-section area A_c (conduction in the solid) plays an important role in the relative contribution of these two channels of heat transfer. The ratio is very large at the microscale, which is directly related to the heat transfer coefficient. The pronounced temperature dependence observed in this study suggests that similar effect can be related to the temperature ratio $\Delta T_m/\Delta T_s$, where ΔT_m is the temperature differential between the heated solid to the ambient medium (solid to fluid medium) and ΔT_s is the temperature differential between the hot and cold end of the specimen (conduction in the solid). This enables us to propose the following empirical relationship for the size and temperature dependence of the heat transfer coefficient [21],

$$h = h_{bulk}\frac{S}{A_c}\frac{\Delta T_m}{\Delta Ts} + \frac{k_{air}}{d_{gap}} \qquad (2.16)$$

where, h_{bulk} is bulk scale heat transfer coefficient, k_{air} is the thermal conductivity of air and d_{gap}(>0) is the distance of the specimen from the nearest solid surface. The second term of Equation 2.16 is predominant for cases where the heated specimen is very closely spaced with a second solid surface. Keeping in mind that the above expression is empirical in nature, we performed three different experiments to determine its validity. Figure 2.6a shows the experimentally obtained temperature profile of a 50 nm thin, 5 μm wide silicon nitride specimen juxtaposed with the predicted values using the heat transfer coefficient given by Equation 2.16. Figure 2.6b shows similar results for a 20 μm thick and 10 μm wide specimen, which is freestanding with no solid surfaces nearby. Figure 2.6c shows a different scenario of specimen that is freestanding, but hangs 2 μm above the device floow. The heat transfer coefficient obtained in this case is very high because the conduction through small air gap plays a dominant role. For all these cases, the remarkable agreement between the experimental and predicted temperature profile suggest the effectiveness of Equation 2.16.

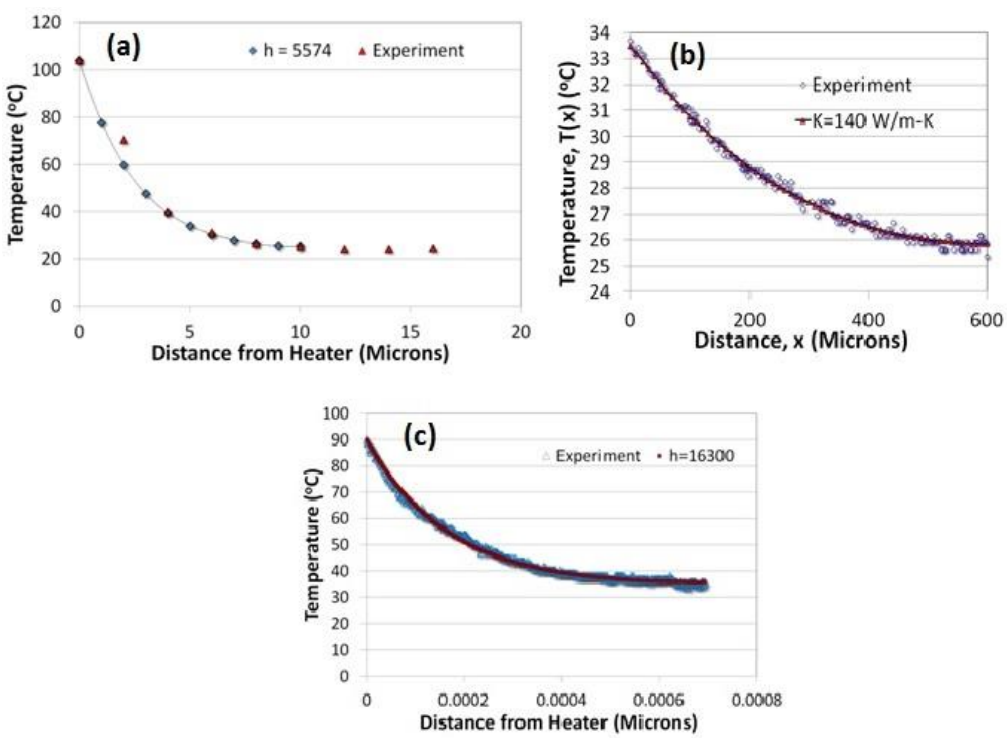

Figure 2.6 Validation of the proposed empirical relation given in equation 2.16 for three different cases, (a) 5 μm wide and 50 nm thick freestanding silicon nitride, (b) 10 μm wide and 20 μm thick silicon specimen with no floor and (c) 10 μm wide and 20 μm thick silicon specimen with a neighboring surface at 2 μm distance

It is important to note that, while the experimental results in this study shown remarkable size and temperature dependence, the most critical influencing factor remains to be the heater geometry. In this paper, the heater is 100 μm long, 10 μm wide and 20 μm deep silicon beam, whose thermal time constant is on the order of tens of micro seconds. According to Equation 2.1, such small thermal time constant leads to the observed heat transfer characteristics dependence on the specimen size. If the specimen were heated using a macro-heater instead, the thermal time constant would be very large, which would reduce the size effect on heat transfer coefficient and this is discussed in detail in the next Chapter.

2.5 Conclusion

This work reports the size and temperature dependence of the heat transfer coefficient and explains the dominating mechanism of the heat transfer process at such size scales. An infrared thermal microscope was used to measure the spatial temperature profiles perpendicular to the microscale specimens, which are integrated with microheaters. Energy balance at the solid-air interface was used to calculate the heat transfer coefficient. The measured heat transfer coefficient varied from 4650 W/m^2K in a 10 μm X 20 μm freestanding specimen to 16,300 W/m^2K for the same specimen with 2 μm away from a neighboring solid surface. The measured values are validated by comparing the measured temperature profile along the length of the specimens with that predicted by the one-dimensional heat transfer. The main contribution of this study is an empirical relation to obtain the heat transfer coefficient for arbitrary specimen size and temperature. It also investigates the effect of medium pressure to find that the temperature dependence remains the same at low pressures but the magnitude of the heat transfer coefficient drops by ~ 4-8% in moderate vacuum from the values at atmospheric pressure.

3. Effect of Heated Zone Size

In microelectronic, micro-electromechanical (MEMS) and other applications involving current flow through narrow resistors, very large density power dissipation takes place. This raises the local temperature, which is cooled by removal of the heat by either convective heat transfer or thermal interface materials. These systems are designed by simulating the heat transfer to determine the limits of safe operating temperature and the role of heater length [2]. In applications with integrated heaters, the heaters are at micro length scales and they form hot spots upon a continuous operation that lead to their premature failure. Cooling involving atomic super-lattice [22, 23] and micro-channels [24] are used for hot spot mitigation in microprocessors.

Whether it is cooling of microprocessors or macroscale objects, the literature considers only the surface to be cooled, and no consideration is given to the active size of the heated zone that is attached to the sample. In other words, the literature tacitly assumes that the cooling dynamics is dominated by the specimen size. This is not categorically true. It is obvious that the Biot number increases as the heater size increases. The relative ratio of the boundary layer thickness to the characteristic length increases as the Biot number decreases [21]. Intuitively, the cooling characteristics of the heater should influence the cooling of the specimen, it being the source of heat to the specimen. For example, a nanoscale specimen connected to a macroscopic heater is exposed to a very thick thermal boundary layer. In addition, even though the specimen has low thermal mass, its cooling rate is dominated by the heaters cooling rate or thermal mass. Interestingly, not a single work has been reported to study this effect, which provides the motivation for the present study. Through experimental design with heater sizes spanning

MEMS to macro scales and keeping the specimen size at the nanoscale, this study presents unambiguous evidence that the size of the heater dominates the heat transfer coefficient associated with these microstructures. Heat transfer coefficient for different heater sizes is evaluated and then validated from temperature profile along a specimen of known thermal conductivity and same structure using these heat sources.

3.1 Experimental Setup

Since the recent studies [4, 10, 21] suggest that the heat transfer coefficient increases at the micro or nanoscale, the role of heaters can be unambiguously quantified if heaters of different sizes can be used to specimens of a certain size (micro or nanoscale). Keeping this argument in mind, heaters of three different sizes are considered for this study: (a) a MEMS heater with 15 μm wide and 20 μm deep resistor size (b) a resistance temperature detector (RTD) element of dimensions 2-3 mm and (c) a Kapton (polyamide film) insulated heater of dimension 1cm X 5cm. Figure 3.1 shows these heating elements. A direct current is passed through each of these heaters and the temperature profile of the quiescent air surrounding the heater is obtained using Infrascope II thermal microscope.

The MEMS heater is fabricated using standard nanofabrication techniques. For validation, the MEMS heater is either integrated with specimen in the device design or the specimen is fabricated separately and then integrated with the MEMS heater. In either case, freestanding micro-fin type specimens are obtained. The nanofabrication process of the device is same as mentioned in Section 2.1. A separate batch of devices is made using thermally grown oxide as the specimen. The fabrication process for these devices also begins with patterning photoresist on a single side polished (SSP) silicon wafer with 300 nm thermally grown oxide layer. An anisotropic etch of the oxide layer using CF_4 chemistry followed by an anisotropic etch of the silicon beneath the specimen makes the sample free standing.

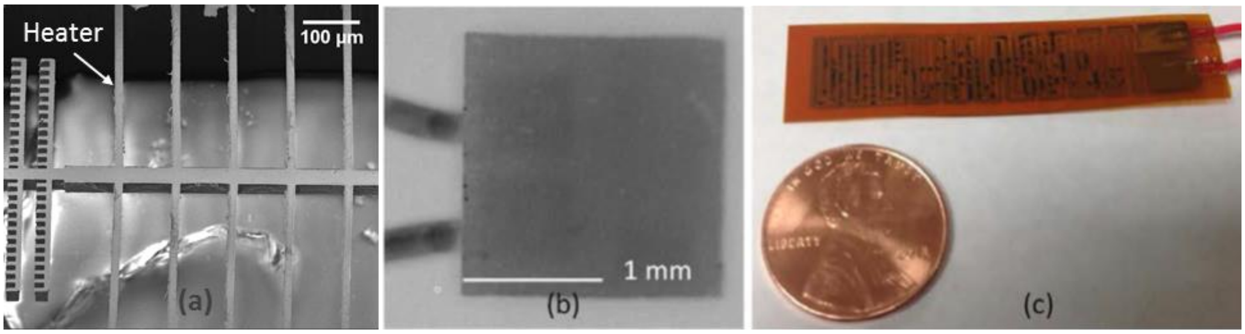

Figure 3.1 Images of the three different heater sizes: (a) MEMS heater (b) RTD heater and (c) Kapton foil heater

3.2 Experimental Procedure

3.2.1 Heat Transfer Coefficient from Thermal Boundary Layer

Heat transfer coefficient is measured by the steady state technique where a direct current is passed through heater of each size. This develops a thermal boundary layer which can be graphically captured using Infrared (IR) microscopy. The temperature distribution in the boundary layer contains the information to evaluate the heat transfer coefficient as described in the mathematical model in Section 2.2.1. Figure 3.1 shows the images from the Infrared microscope of the MEMS, RTD and Kapton heaters respectively. In a typical experiment, these heaters are activated in ambient environment to generate a thermal boundary layer. The thermal boundary layer is then visualized and quantified with the IR microscope.

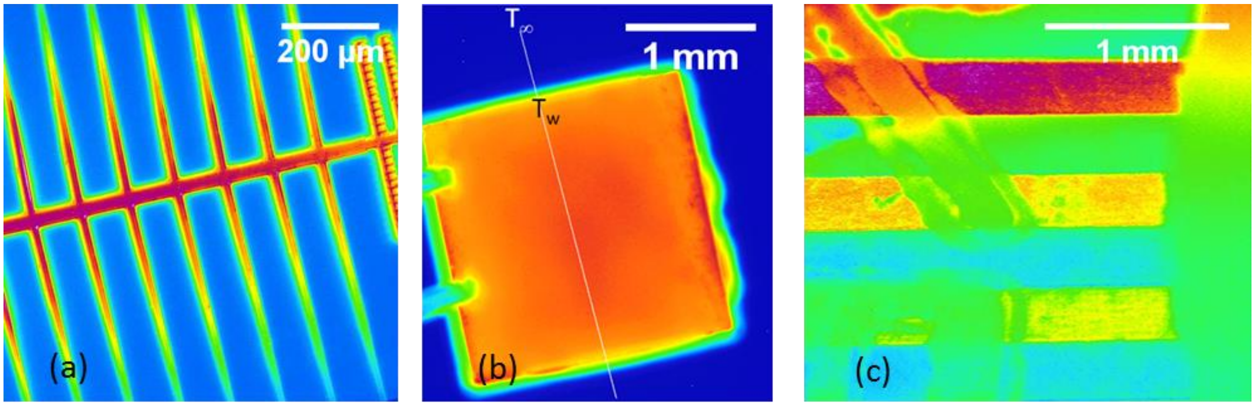

Figure 3.2 Infrared micrograph of (a) MEMS (b) RTD and (c) Kapton foil heaters

3.2.2 Procedure for Validation of Experimental Results

To validate the heat transfer coefficient measurement described above, a second set of experiments is carried out. Here, micro-fin shaped specimens with rectangular cross-section of material with known thermal conductivity and dimensions are heated with the heaters. The IR microscope is again used to map the temperature profile, this time on the solid specimen and not the thermal boundary layer. An approximation of one-dimensional conduction along the length of the micro-fin specimen together with heat loss through convection allows it to be modeled by the Fourier equation. This model is similar to that described in the Section 2.3.2, where it is shown to involve two parameters: the thermal conductivity of specimen 'k_s' and the heat transfer coefficient 'h'. Usage of known materials (silicon and silicon dioxide) as the specimen allows obtaining the heat transfer coefficient, so that these values can be compared with that measured from the thermal boundary layer technique. Figure 3.3 shows two examples of this experimental configuration. In the first example, a MEMS type line heater (not an array as shown in Figure 3.1) is shown to heat a microscale silicon beam (2 micron thick). The second example shows a cantilevered thermally grown silicon dioxide beam (300 nm thick) heated by a RTD heater. Since these materials are well characterized for their thermal conductivity (140 W/m-K and 1.2

W/m-K respectively) [25, 26], an energy balance model given in Section 2.3.2 can be used to calculate the heat transfer coefficient values that can be cross-checked against the results obtained from Section 3.2.1.

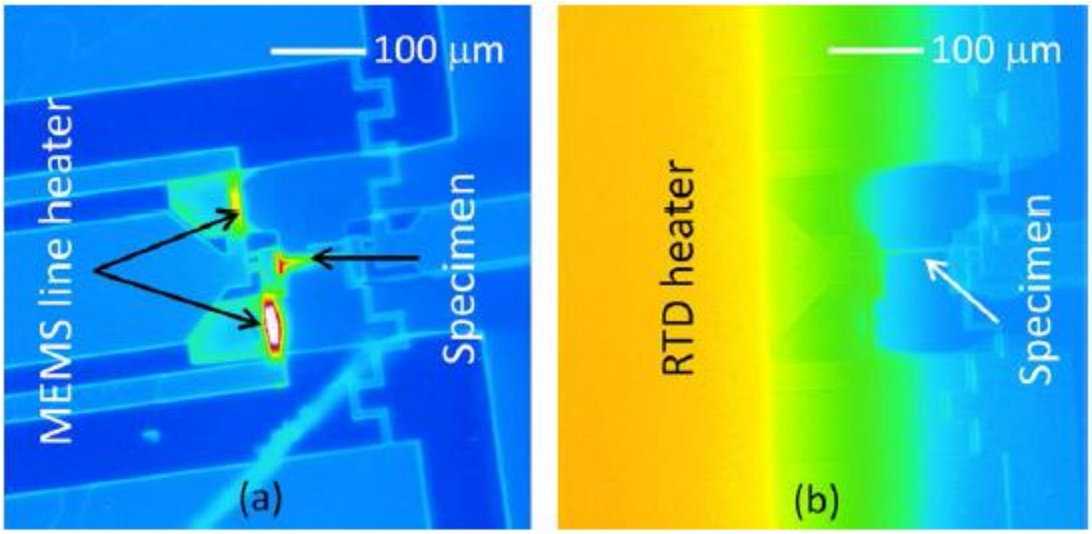

Figure 3.3 Infrared micrograph of (a) single crystal silicon and (b) thermally grown silicon oxide heated by MEMS and RTD heaters respectively

3.3 Experimental Results and Validation

Figure 3.4 shows the experimental data on the steady state spatial temperature profile of the thermal boundary layer according to Equation 2.4. The slope of the plots shown on multiplication with the thermal conductivity of air, gives the heat transfer coefficient as per Equation 2.7. The thermal conductivity of air, k_{air} is taken as 0.024 W/m-K. This yields h value of 3200 W/m^2-K for the MEMS heater and 110 W/m^2-K for the RTD element. For the Kapton heater (a bulk object with macroscopic physical dimensions), the transient technique gives value of h in the range of 10-15 W/m^2-K which is in good agreement with the literature for macroscopic objects.

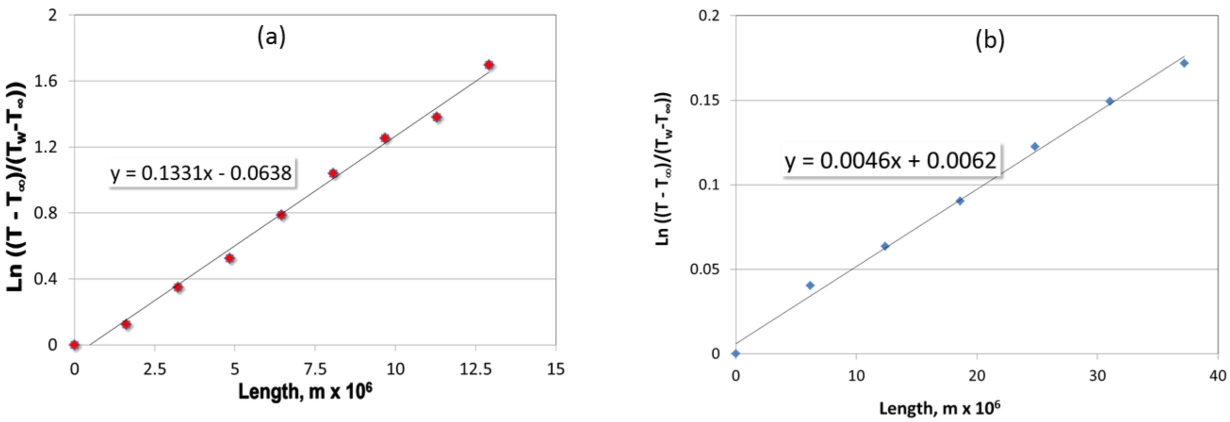

Figure 3.4 Temperature profile in thermal boundary layer of (a) MEMS and (b) RTD heater elements

The validation of the experimental results was done using a silicon specimen for the case of MEMS heater and silicon dioxide specimen (thermally grown) for RTD and Kapton heaters. Section 2.3.1 has already reported the dependence of heat transfer coefficient on temperature of the specimen using a silicon sample with a MEMS heater. The h value was on the order of 3000 W/m^2-K near the area of sample close to the heater that agrees with the above evaluated value for MEMS heater. Figure 3.5 shows the experimental and model predicted temperature profiles along the length of the thermally grown silicon dioxide samples (5 µm wide and 100 µm long) for both the cases of RTD and Kapton foil heaters.

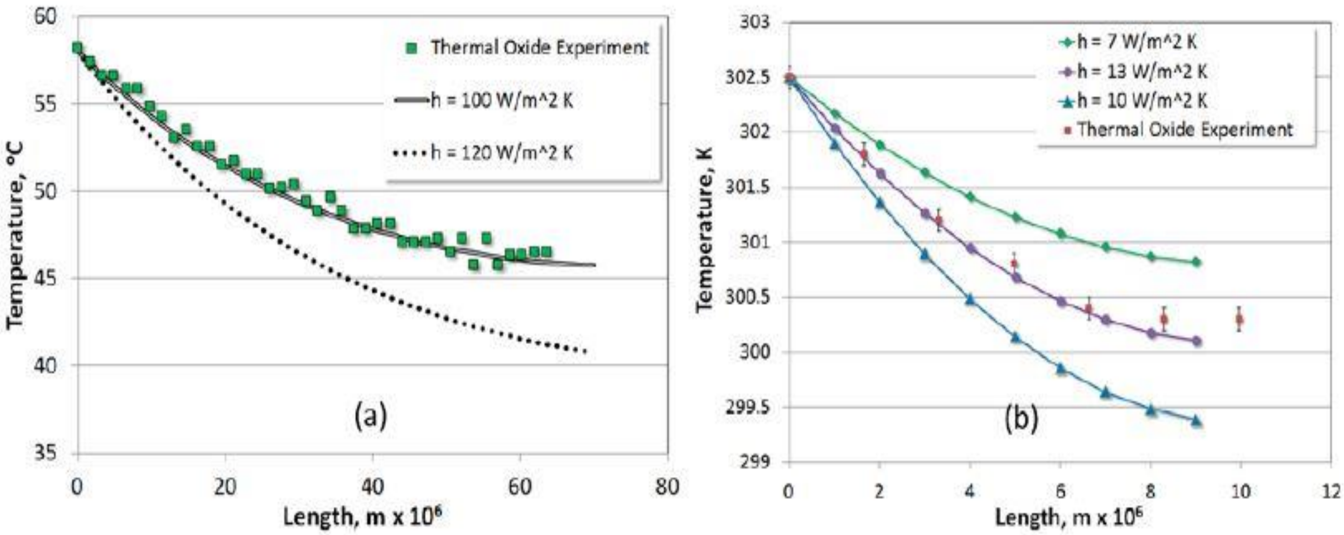

Figure 3.5 Validation of heat transfer coefficient using temperature profiles in thermal oxide specimens using (a) RTD and (b) Kapton foil heaters

It is evident from Figure 3.5 that heat transfer coefficient h = 100 W/m^2-K and h = 13 W/m^2-K fits the experimental readings from the Infrared microscope for heating with RTD element and Kapton heater respectively. These agree very well with estimated heat transfer coefficient values discussed above.

3.4 Discussion and Conclusion

Two different kinds of experiments are performed to rigorously show that unlike the known size effect of specimen on the heat transfer coefficient, it is the size of the heat generation zone that dominates the dependence of heat transfer coefficient. In the first set of experiments, the heat transfer coefficient is measured from the heat generators of micron, meso (RTD) and macro (Kapton foil) scales. The micron scale structures showed fastest response to heating and cooling and also had he largest value of heat transfer coefficient, h = 3200 W/m^2-K. In comparison, the meso and macro scale heaters are very slow and the macro scale heater displayed the slowest time response. These two heaters yielded heat transfer coefficient values of 100 W/m^2-K and 13 W/m^2-K. To show that heater size dominates specimen size, a second set of experiments are conduced where the heat transfer coefficient is obtained from the spatial temperature profile of microscale specimens with known thermal conductivity values using the energy balance approach. The excellent agreement between both the results indicates that heater size dominates the mode and magnitude of the convective heat transfer at smaller scales.

The same conclusion can be achieved from a different perspective, such as the characteristic length scale dependence of the cooling rate. It is well known that smaller systems (heater or specimen) have very small thermal mass and get cooled very fast by heat loss due to the free convection. For such specimens, the heater size can be very important. When they are physically attached to bulky heaters, their cooling dynamics are governed by the cooling rate of the heater.

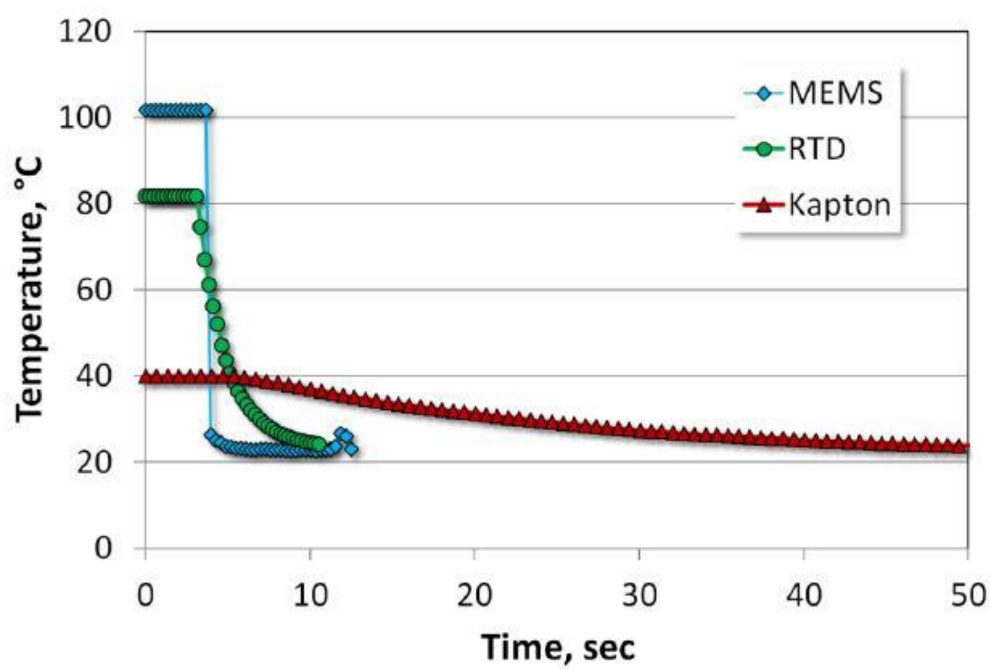

Figure 3.6 Cooling curves of surrounding ambient air for the three different heater sizes

Figure 3.6 shows that the cooling rate varies with the size of heater, highest being for a MEMS heater and the least for Kapton heater. This implies that a sample specimen will show largest value of heat transfer coefficient for MEMS heater, intermediate value for the RTD element and the least for the case of Kapton heater. The size of the heater strongly influences the heat transfer coefficient. Besides this, the heat transfer coefficient of a specimen may not necessarily be the same when evaluated by steady state technique and the transient technique due to the governance of associated heater in the transient technique as shown above.

REFERENCES

1. Maghsoudi, E. and M.J. Martin, *Scaling of Thermal Positioning in Microscale and Nanoscale Bridge Structures.* Journal of Heat Transfer-Transactions of the Asme, 2012. **134**(10).

2. Banerjee, S., et al., *Natural convection in a bi-heater configuration of passive electronic cooling.* International Journal of Thermal Sciences, 2008. **47**(11): p. 1516-1527.

3. Guo, Z.Y. and Z.X. Li, *Size effect on single-phase channel flow and heat transfer at microscale.* International Journal of Heat and Fluid Flow, 2003. **24**(3): p. 284-298.

4. Kim, K.J. and W.P. King, *Thermal conduction between a heated microcantilever and a surrounding air environment.* Applied Thermal Engineering, 2009. **29**(8-9): p. 1631-1641.

5. Wang, Z.L. and D.W. Tang, *Investigation of heat transfer around microwire in air environment using 3 omega method.* International Journal of Thermal Sciences, 2013. **64**: p. 145-151.

6. Peirs, J., et al., *Scale effects and thermal considerations for micro-actuators*, in *1998 Ieee International Conference on Robotics and Automation, Vols 1-4*. 1998, Ieee: New York. p. 1516-1521.

7. Zhu, R., et al., *Micromachined gas inertial sensor based on convection heat transfer.* Sensors and Actuators a-Physical, 2006. **130**: p. 68-74.

8. Strelcov, E., Y. Lilach, and A. Kolmakov, *Gas Sensor Based on Metal-Insulator Transition in VO2 Nanowire Thermistor.* Nano Letters, 2009. **9**(6): p. 2322-2326.

9. Strnad, J. and A. Vengar, *Stefan's measurement of the thermal conductivity of air.* European Journal of Physics, 1984. **5**(1): p. 9.

10. Hu, X.J., A. Jain, and K.E. Goodson, *Investigation of the natural convection boundary condition in microfabricated structures.* International Journal of Thermal Sciences, 2008. **47**(7): p. 820-824.

11. Ozsun, O., et al., *On heat transfer at microscale with implications for microactuator design.* Journal of Micromechanics and Microengineering, 2009. **19**(4).

12. Cheng, C., et al., *Heat Transfer across the Interface between Nanoscale Solids and Gas.* ACS Nano, 2011. **5**(12): p. 10102-10107.

13. Guo, Z.-Y. and Z.-X. Li, *Size effect on microscale single-phase flow and heat transfer.* International Journal of Heat and Mass Transfer, 2003. **46**(1): p. 149-159.

14. Giani, A., et al., *Thermal model of thin film anemometer.* Microelectronics Journal, 2002. **33**(8): p. 619-625.

15. Ramanan, S. and R.G. Yang, *Effect of gas rarefaction on the performance of submicron fins.* Applied Physics Letters, 2009. **94**(14).

16. van Rij, J., T. Ameel, and T. Harman, *The effect of viscous dissipation and rarefaction on rectangular microchannel convective heat transfer.* International Journal of Thermal Sciences, 2009. **48**(2): p. 271-281.

17. Incropera, F.P.D., D.P., *Introduction to Heat Transfer*, J.W. Sons, Editor 2002: New York.

18. Carlomagno, G.M. and G. Cardone, *Infrared thermography for convective heat transfer measurements.* Experiments in Fluids, 2010. **49**(6): p. 1187-1218.

19. Hetsroni, G., et al., *Infrared temperature measurements in micro-channels and micro-fluid systems.* International Journal of Thermal Sciences, 2011. **50**(6): p. 853-868.

20. Roldan, C., et al., *A laboratory experiment for measuring the free convection heat transfer coefficient of a plane metal plate.* European Journal of Physics, 1993. **14**(3): p. 128.

21. Alam, M.T., et al., *Structural size and temperature dependence of solid to air heat transfer.* International Journal of Thermal Sciences, 2013. **73**: p. 1-7.

22. Zhang, Y., et al., *Experimetnal characterization of bonded microcoolers for hot spot removal*. Advances in Electronic Packaging 2005, Pts A-C. 2005, New York: Amer Soc Mechanical Engineers. 2185-2193.

23. Solbrekken, G.L., et al., *Use of superlattice thermionic emission for "hot spot" reduction in a convectively-cooled chip*. Itherm 2004, Vol 2, ed. K. Ramakrishna, et al. 2004, New York: Ieee. 610-616.

24. Chauhan, A., et al., *Hot Spot Mitigation using Single-Phase Microchannel cooling for Microprocessors*, in *2010* 12th IEEE Intersociety Conference on Thermal and Thermomechanical Phenomena in Electronic Systems. 2010, IEEE: New York.

25. Yamasue, E., et al., *Thermal conductivities of silicon and germanium in solid and liquid states measured by non-stationary hot wire method with silica coated probe.* Journal of Crystal Growth, 2002. **234**(1): p. 121-131.

26. Ju, Y.S. and K.E. Goodson, *Process-dependent thermal transport properties of silicon-dioxide films deposited using low-pressure chemical vapor deposition.* Journal of Applied Physics, 1999. **85**(10): p. 7130-7134.